GSI

GSI-Preprint-97- 40
August 1997

MASSES AND RADII OF SPHERICAL NUCLEI CALCULATED IN VARIOUS MICROSCOPIC APPROACHES

Z. Patyk. A. Baran, J. F. Berger, J. Dechargé, J. Dobaczewski, P. Ring, A. Sobiczewski

(Submitted to Phys. Rev. C)

Gesellschaft für Schwerionenforschung mbH
Planckstraße 1 • D-64291 Darmstadt • Germany
Postfach 11 05 52 • D-64220 Darmstadt • Germany

Masses and radii of spherical nuclei calculated in various microscopic approaches

Z. Patyk[1,2], A. Baran[3], J.F. Berger[4], J. Dechargé[4], J. Dobaczewski[5], P. Ring[6] and A. Sobiczewski[1,2]

[1]Soltan Institute for Nuclear Studies, Hoża 69, PL-00-681 Warsaw, Poland
[2]GSI, D-64220 Darmstadt, Germany
[3]Institute of Physics, M.Curie–Skłodowska University, PL-20-031 Lublin, Poland
[4]Centre d'Etudes de Bruyères-le-Châtel, F-91680 Bruyères-le-Châtel, France
[5]Institute of Theoretical Physics, Warsaw University, Hoża 69, Warsaw, Poland
[6]Physik Department, Technische Universität München, D-85747 Garching, Germany

The quality of the description of nuclear masses and charge radii, calculated in various microscopic approaches, is studied. The Hartree-Fock-Bogoliubov (HFB), Extended Thomas-Fermi model with Strutinski Integral (ETFSI), Relativistic Mean Field (RMF) and Macroscopic-Microscopic (MM) approaches are considered. In the HFB approximation, both finite-range (Gogny) and zero-range (Skyrme) effective forces are used. Spherical even-even nuclei (116 nuclides), from light (A=16) to heavy (A=220) ones, with known experimental mass are chosen for the study. A general result is that the best description of masses of considered nuclei is obtained in the MM and ETFSI approaches, while the best charge radii are obtained within the RMF and ETFSI approximations. The behaviour of nuclear masses and radii, when one moves far off the β-stability line, is also studied.

PACS numbers: 21.10.Dr, 21.10.Ft, 21.10.Gv, 21.60.Jz

1 Introduction

Recently one witnesses an impressive increase in the number of nuclei far from stability, for which the masses have been measured [1,2]. This tendency is expected to be continued, due to a fast progress in the development of techniques of radioactive beams (e.g. [3–5]). Also the accuracy of measurements of nuclear masses is being significantly improved. For example, the use of the Penning trap leads to accuracies

of about 10 keV [6]. Progress in measuring nuclear radii is also large (e.g. [7,8]), and the increase in quality and quantity of available data constitutes a formidable challenge for the nuclear structure theory.

The objective of the present paper is to study these two basic properties of nuclei, masses and radii, and address the question how well they can be described by the present-day microscopic approaches. Such an analysis may also serve as a starting point to improve these approaches. We also aim at predicting the behaviour of masses and radii in nuclei far from the β-stability line. Difference in predictive powers of various theoretical methods can give us one of the best indications on which of them is more reliable. This may serve as a guideline not only for future experiments but also for the astrophysical applications which often require knowledge of data which will not be easily accessible in the nearest future.

We limit our study to microscopic approaches, i.e., those which derive nuclear properties from the fact that nuclei are built of interacting neutrons and protons. Among these, we employ theories which use the effective two-body interactions or Lagrangians, as the self-consistent Hartree-Fock-Bogoliubov (HFB) approach with zero-range (Skyrme) and finite-range (Gogny) effective interactions, or the Relativistic Mean Field (RMF) theory. We also present results obtained within the Extended Thomas-Fermi model with Strutinski Integral (ETFSI), which combines the features of the self-consistent Hartree-Fock approach with those of the Macroscopic-Microscopic (MM) approximation, as well as those obtained within the MM models, themselves.

In the present study, we consider only the spherical nuclei; 116 even-even nuclides with the mass numbers $A \geq 16$, known experimental masses, and which are close enough to magic numbers of protons and neutrons to be considered spherical, are taken. The paper is an extension of our previous work [9].

Our paper is organized in the following way. Theoretical approaches used in the paper are summarized in sect. II. The results of calculations and their discussion are presented in sect. III, while sect. IV gives the conclusions drawn from our study.

2 Theoretical approaches

In the present Section, we very briefly present essential elements of the theoretical approaches used. Without going into any details, we aim at stressing generic similarities and differences between the theories which are important in trying to understand similarities and differences between the obtained results.

2.1 HFB with the Skyrme force

The Skyrme type [10] force used in the present study has the following standard form (e.g. [11–13])

$$\begin{aligned} v(\mathbf{r}_{12}) &= t_0\,(1+x_0P_\sigma)\delta(\mathbf{r}_{12}) + \tfrac{1}{2}t_1(1+x_1P_\sigma)[\mathbf{k}_{21}^2\delta(\mathbf{r}_{12}) + \delta(\mathbf{r}_{12})\mathbf{k}_{12}^2] \\ &+t_2(1+x_2P_\sigma)\mathbf{k}_{21}\cdot\delta(\mathbf{r}_{12})\mathbf{k}_{12} + \tfrac{1}{6}t_3(1+x_3P_\sigma)\rho^\alpha(\mathbf{R})\delta(\mathbf{r}_{12}) \\ &+iW_0\boldsymbol{\sigma}\cdot[\mathbf{k}_{21}\times\delta(\mathbf{r}_{12})\mathbf{k}_{12}], \end{aligned} \tag{1}$$

where $\mathbf{r}_{12} = \mathbf{r}_1 - \mathbf{r}_2$ is the vector of relative position of interacting nucleons, $\mathbf{k}_{12} = (\boldsymbol{\nabla}_1 - \boldsymbol{\nabla}_2)/2i$, $\mathbf{k}_{21} = (\boldsymbol{\nabla}_2 - \boldsymbol{\nabla}_1)/2i$ are the respective vectors of relative momentum and are acting to the right and to the left, respectively, $\mathbf{R} = (\mathbf{r}_1 + \mathbf{r}_2)/2$, $\boldsymbol{\sigma} = \boldsymbol{\sigma}_1 + \boldsymbol{\sigma}_2$, P_σ is the spin-exchange operator, and t_i, x_i, $(i = 0, 1, 2, 3)$, W_0 and α are adjustable parameters. (One should note here that the parameter t_3 of [11] is defined as 1/6 of that in eq. (1), the latter equation being, however, a more widely accepted definition.)

Out of all versions of the interaction exploited up to now, we choose the following three. One is the widely and for a long time studied interaction SIII (cf. e.g. [13,14]). The second one is the interaction SkM* [11] which is a modification of the earlier interaction SkM [15] and has been introduced to better reproduce the experimental binding energies and fission barriers of nuclei. The third variant of the interaction is the SkP one, developed in [16] to obtain a good description of pairing correlations within the HFB approach, and, simultaneously, preserving the same accuracy in reproducing other properties of nuclei reached with earlier variants of the force.

Table I specifies the parameters of the interaction for all three variants. Recently, also new sets of parameters of the Skyrme force, specially devised for neutron-rich nuclei, have been proposed [17,18].

The three Skyrme forces, taken by us, are used for the calculations in the particle-hole (p-h) channel, i.e., for the generation of the mean field. For each force, however, three different interactions are used for the calculations in the particle-particle (p-p) channel [19], i.e., for the generation of the pairing correlations. The first interaction is just the same as that used in the p-h channel. The second is the contact δ force

$$V^\delta(\mathbf{r}_{12}) = V_0\delta(\mathbf{r}_{12}) \tag{2}$$

and the third is the δ force with the strength dependent on nuclear density

$$V^{\delta\rho}(\mathbf{r}_{12}) = (V_0 + \frac{1}{6}V_3\rho^\gamma)\delta(\mathbf{r}_{12}). \tag{3}$$

Thus, for each standard force, three effective interactions are finally used. They are denoted [19], e.g., in the case of the SIII force, by SIII, SIII$^\delta$ and SIII$^{\delta\rho}$, respectively.

Table I. Values of the parameters of the Skyrme interactions: SIII, SkM*, SkP and SkSC4

Param.	Units	SIII	SkM*	SkP	SkSC4
t_0	MeV·fm^3	-1128.75	-2645.00	-2931.70	-1789.420
t_1	MeV·fm^5	395.00	410.00	320.62	283.467
t_2	MeV·fm^5	-95.00	-135.00	-337.41	-283.467
t_3	MeV·fm^6	14000.00	15595.00	18708.97	12782.300
x_0	–	0.45	0.09	0.29215	0.790
x_1	–	0.00	0.00	0.65318	-0.500
x_2	–	0.00	0.00	-0.53732	-0.500
x_3	–	1.00	0.00	0.18103	1.13871
W_0	MeV·fm^5	120.00	130.00	110.00	124.877
α	–	1.00	1/6	1/6	1/3
Ref.	–	[13, 14]	[11]	[16]	[28]

A motivation for introducing the interactions, eqs. (2) and (3), in the p-p channel is that only the SkP force is chosen in such a way as to give reasonable pairing correlations. The SIII and SkM* forces, however, are repulsive in the p-p channel and lead to a vanishing pairing. The parameters of the interactions (2) and (3) are taken the same as in [19], where they were adjusted to reproduce the experimental neutron pairing gap for the nucleus ^{119}Sn.

We use the approach in which the hamiltonian is treated in the spatial-coordinate representation. The corresponding HFB equations take the form of two coupled differential equations, which are solved numerically in the way described in [16]. An advantage of this approach is that it properly takes into account the particle continuum states, and therefore, makes the approach also applicable to nuclei far from the β-stability line. A disadvantage is a necessity to use cut-off parameters in the summation of nuclear densities, which is a consequence of the unphysically large strength of the Skyrme force for high particle momenta (cf. the discussion in [20]).

2.2 HFB with the Gogny force

The finite-range Gogny force has been specially devised (similarly as the zero-range SkP force) to describe the pairing properties simultaneously with the mean field, within the HFB formalism. With this force, one avoids divergencies in the pairing calculations, in contrast with the zero-range forces, for which the energy cut-off is

necessary and plays the role of an additional parameter, as already mentioned above. However, the resulting non-locality of the mean fields precludes a solution in spatial coordinates and does not allow for analyzing the coupling to continuum states.

The Gogny force has been proposed in [21] and has the form [21,22]

$$\begin{aligned} v(\mathbf{r}_{12}) &= \textstyle\sum_{i=1,2}(W_i + B_i P_\sigma - H_i P_\tau - M_i P_\sigma P_\tau) e^{-\mathbf{r}_{12}^2/\mu_i^2} \\ &+ t_3(1 + x_3 P_\sigma)\rho^\alpha(\mathbf{R})\delta(\mathbf{r}_{12}) + iW_{LS}\boldsymbol{\sigma}\cdot[\boldsymbol{\nabla}_{21}\times\delta(\mathbf{r}_{12})\boldsymbol{\nabla}_{12}], \end{aligned} \tag{4}$$

where P_σ and P_τ are the spin and isospin exchange operators, respecively, $\boldsymbol{\nabla}_{12} = \boldsymbol{\nabla}_1 - \boldsymbol{\nabla}_2$, and the other notation is the same as in eq.(1). The quantities μ_i, W_i, B_i, H_i, M_i (i=1,2) and $t_3, x_3, W_{\rm LS}$ are adjustable parameters, together 13 parameters. Thus, the central force has two parts. One is composed of two Gaussian functions (with a short and intermediate ranges) and is independent of the density. The other is of zero range, depends on the density and is of the same form as that in the Skyrme force. It is needed to get the property of saturation. The spin-orbit term is also of the same form as that in the Skyrme force.

In all calculations performed up to now with the Gogny force, two variants of the parameters, D1 and D1S, have been used. The D1S variant is a modification of the earlier force D1 to better reproduce the fission barriers [23], the heights of which were overestimated with the D1 force. Since the study [23], in which the D1S force has been introduced, only this force is used in all calculations. We also employ it in this paper. The parameters of it [24] are given in Table II.

Table II. Values of the parameters of the Gogny interaction D1S [24]

	W_i	B_i	H_i	M_i	μ_i	t_3	x_3	W_{LS}	α
	MeV	MeV	MeV	MeV	fm	MeV	–	MeV	–
i=1	-1720.30	1300.00	-1813.53	1397.60	0.7	1390.60	1.00	130	1/3
i=2	103.64	-163.48	162.81	-223.93	1.2				

The success of the Gogny force is that it is able to reproduce a wide range of nuclear properties with one set (D1S) of its parameters, as discussed in [25,26].

The HFB equations are solved by diagonalization in the harmonic oscillator basis; 13 oscillator shells are taken for the lightest nuclei, like Ca, and 17 shells for the heaviest ones, like Pb.

2.3 Extended Thomas-Fermi model with Strutinski Integral

This approach is something between the self-consistent Hartree-Fock (HF) approximation and the Macroscopic-Microscopic (MM) approach. It uses the expansion of the HF energy (which is a functional of the HF density $\rho_{\rm HF}$) in powers of

$$\delta\rho = \rho_{\rm HF} - \tilde{\rho}, \tag{5}$$

where $\tilde{\rho}$ is a smooth approximation to $\rho_{\rm HF}$. The expansion retains only the linear term in $\delta\rho$, leading to the Strutinski energy theorem

$$E[\rho_{\rm HF}] \approx E[\tilde{\rho}] + \sum_{i,q} \tilde{\epsilon}_i^q - tr(\tilde{h}\tilde{\rho}), \tag{6}$$

where $\tilde{h}$ is the smooth single-particle hamiltonian generated from $\tilde{\rho}$ by the effective nucleon-nucleon interaction, $\tilde{\epsilon}_{\rm i}^{\rm q}$ are the eigenvalues of $\tilde{h}$, q stands for p (protons) or n (neutrons) and the summation over i extends over all occupied single-particle states. For the interaction, the Skyrme force, eq.(1), is taken. Its parameters were treated as independent ones in their fit to experimental masses. Their final values [27,28], labeled by SkSC4, are shown in Table I. The effective mass $m_{\rm q}^*$ of a nucleon is taken to be equal to its real mass $m_{\rm q}$.

The Thomas-Fermi energy is adopted for $E[\tilde{\rho}]$ in eq. (6), with $\tilde{\rho}$ taken in the simple Fermi form

$$\tilde{\rho}_{\rm q}(r) = \tilde{\rho}_{\rm q0}/[1 + exp(r - C_{\rm q})/a_{\rm q}], \tag{7}$$

where parameters $C_{\rm q}$ and $a_{\rm q}$ are determined by minimizing $E[\tilde{\rho}]$.

Formula (6) for the energy has the form of that used in the MM approach. There is, however, an important difference. In the MM approach, the macroscopic (smooth) part is not connected with the microscopic (shell correction) part. In distinction to that, the smooth energy $E[\tilde{\rho}]$ in eq. (6) is calculated with the same $\tilde{\rho}$ which appears in the shell correction. Also the smooth part of the sum of the single-particle energies $tr(\tilde{h}\tilde{\rho})$ (Strutinski integral) is calculated here without using the Strutinski smearing prescription. This makes the ETFSI approach applicable also to nuclei close to the drip lines.

The pairing interaction is treated by the BCS method with the pairing force taken in the form of eq. (2). The same V_0 is assumed for protons and neutrons and fitted, together with the Skyrme-force parameters, to best reproduce experimental masses. The result is: $V_0 = -220.0$ MeV $\cdot$ fm^3.

The charge radius of a nucleus is calculated as

$$< r^2 >_{\rm ch}^{1/2} = \{< r^2 >_{\rm p} + s_{\rm p}^2\}^{1/2}, \tag{8}$$

where

$$< r^2 >_{\rm p} = \int \tilde{\rho}_{\rm p}(\mathbf{r}) r^2 d\mathbf{r} \tag{9}$$

and $s_{\rm p} = 0.8$ fm is the rms radius of the charge distibution of proton.

A detailed description of the ETFSI approach is given in [27,28] and in references quoted therein.

2.4 Relativistic Mean Field approach

This approach is based on a Lagrangian which describes the interaction of nucleons by exchange of mesons and photons in the Lorentz-invariant way. The Lagrangian density has the form [29–33]

$$\begin{aligned} \mathcal{L} \ &= \bar{\psi}(i\gamma_\mu \partial^\mu - M)\psi + \tfrac{1}{2}\partial_\mu \sigma \partial^\mu \sigma - U(\sigma) - \tfrac{1}{4}\Omega_{\mu\nu}\Omega^{\mu\nu} \\ &+ \tfrac{1}{2} m_\omega^2 \omega_\mu \omega^\mu - \tfrac{1}{4}\mathbf{R}_{\mu\nu}\mathbf{R}^{\mu\nu} + \tfrac{1}{2} m_\rho^2 \boldsymbol{\rho}_\mu \boldsymbol{\rho}^\mu - \tfrac{1}{4} F_{\mu\nu} F^{\mu\nu} \\ &- g_\sigma \bar{\psi}\sigma\psi - \ g_\omega \bar{\psi}\gamma_\mu \psi \omega^\mu - \ g_\rho \bar{\psi}\gamma_\mu \boldsymbol{\tau} \psi \boldsymbol{\rho}^\mu \ - \ e\bar{\psi}\gamma_\mu \psi A^\mu, \end{aligned} \tag{10}$$

where ψ is the nucleon (Dirac spinor) field, σ is the scalar, ω^μ is the isoscalar-vector and $\boldsymbol{\rho}^\mu$ is the isovector-vector meson fields, with the masses m_σ, m_ω and m_ρ, and the coupling constants g_σ, g_ω and g_ρ, respectively; A^μ is the electromagnetic field. The quantities $\Omega^{\mu\nu}, \mathbf{R}^{\mu\nu}$ and $F^{\mu\nu}$ are tensors of the respective fields. The potential $U(\sigma)$ for the scalar meson σ is assumed in the form

$$U(\sigma) \ = \frac{1}{2} m_\sigma^2 \sigma^2 \ + \ \frac{1}{3} g_3 \sigma^3 \ + \ \frac{1}{4} g_4 \sigma^4, \tag{11}$$

i.e. with two self-coupling terms (non-linearity).

The coupled Dirac and Klein-Gordon equations, corresponding to the Lagrangian (10), are solved in the self-consistent Hartree way. The basis consisting of 20 oscillator shells has been used when solving the equations.

Nine constants: M,$m_\sigma, m_\omega, m_\rho, g_\sigma, g_\omega, g_\rho, g_3$ and g_4 are treated as parameters of the theory. Three sets of these parameters: NL1 [34], NL2 [35] and NL3 [36] are taken for the calculations. Two of them, NL1 and NL2, are already discussed for a longer time. The third one, NL3, is a very recent set. The parameters of these three sets are given in Table III, for convenience of the reader. The pairing interaction characterized by the energy gap $\Delta = 12A^{-1/2}$ has been used.

Table III. Values of the parameters of the RMF approach

Param.	Units	NL1	NL2	NL3
M	MeV	938.0	938.0	939.0
m_σ	MeV	492.25	504.89	508.194
m_ω	MeV	795.359	780.0	782.501
m_ρ	MeV	763.0	763.0	763.0
g_σ	–	10.138	9.111	10.217
g_ω	–	13.285	11.493	12.868
g_ρ	–	4.976	5.507	4.474
g_3	fm^{-1}	-12.172	-2.304	-10.431
g_4	–	-36.265	13.783	-28.885
Ref.	–	[34]	[35]	[36]

2.5 Macroscopic-microscopic model

In this study, we use two recent versions of the macroscopic-microsopic model. One is the Finite-Range Droplet Model (FRDM) [37] and the other is the Thomas-Fermi (TF) model [38].

The macroscopic part of FRDM is an extension of the original droplet model [39] to improve description of the average nuclear properties. The microscopic part is the Strutinski shell correction, based on the folded-Yukawa single-particle potential. Nine parameters of the model are fitted to the ground-state masses of 1654 nuclei (with the proton number $Z \geq 8$ and the neutron number $N \geq 8$) and to 28 fission-barrier heights. The model is described in detail in [37].

The macroscopic part of mass of the TF model is based on a (generalized Seyler-Blanchard) effective nucleon-nucleon interaction, which is of the Yukawa type with the strength dependent on the average density of interacting nucleons and on their relative momentum. Six of the seven parameters of the interaction are fitted to 1654 ground-state masses of nuclei with $Z, N \geq 8$. The microscopic part is taken the same as in FRDM [37] for nuclei with $Z, N \geq 30$. For lighter nuclides, this part is taken in a semiempirical form with additional parameters fitted to masses of these light nuclei. As a result, the model describes masses of all nuclides, starting from that with $Z, N = 1$. Details of it are given in [38].

3 Results and discussion

3.1 Masses

Table IV gives the rms values of the difference between the calculated and experimental masses. The differences are calculated for 116 even-even spherical nuclei, from ^{16}O to ^{220}Th, for which the experimental masses are known. The table is very similar to that given by us earlier [9]. Only in the RMF case, the NLSH variant [40] of the parameters has been presently replaced by the more recent variant NL3 [36]. All HFB and RMF masses are calculated by us, the ETFSI results are taken from [28] and the MM masses are taken from [37] in their FRDM and FRLDM variants, and from [38] in their TF variant of the smooth part of the mass. As the experimental values, the masses evaluated by Audi and Wapstra [41] are used.

Table IV. Mass rms deviations in MeV

SIII:	4.74	SkP:	2.37	SkM*:	6.32
SIII$^{\delta}$:	3.07	SkP$^{\delta}$:	2.53	SkM*$^{\delta}$:	5.36
SIII$^{\delta\rho}$:	2.26	SkP$^{\delta\rho}$:	2.32	SkM*$^{\delta\rho}$:	4.74
Gogny:	2.07				
RMF(NL1):	3.94	RMF(NL2):	11.24	RMF(NL3):	2.48
ETFSI:	0.80				
MM(FRDM):	0.65	MM(FRLDM):	0.76	MM(TF):	0.57

One can see in Table IV that the smallest deviations from experimental masses are obtained in the MM approach. Within the HFB approximation, the best results are obtained with the Gogny force. Among the Skyrme forces, the best results are obtained in the SkP case. The results obtained with the interaction modified in the p-p channel, SkP$^{\delta\rho}$, are only very little better than those with the original force SkP, and the SkP$^{\delta}$ results are even slightly worse. This differs from the case of the SIII (and also SkM*) force, for which the variant SIII$^{\delta\rho}$ is much better than SIII$^{\delta}$. Results labeled as SIII and SkM* correspond to vanishing pairing correlations, as discussed in sect. 2.1, and are therefore much worse. The results obtained within the RMF theory strongly depend on the variant of the parameters used. They are very poor with the NL2 set, while they are quite good with the very recent variant NL3.

Figure 1 shows the dependence of the deviations from experimental masses on the neutron number N. Isotopes of six elements with Z=20(Ca), 38(Sr), 50(Sn), 62(Sm), 82(Pb) and 90(Th) are taken. These are the nuclides, the proton number Z or neutron number N of which are magic or close to magic numbers, as these nuclei

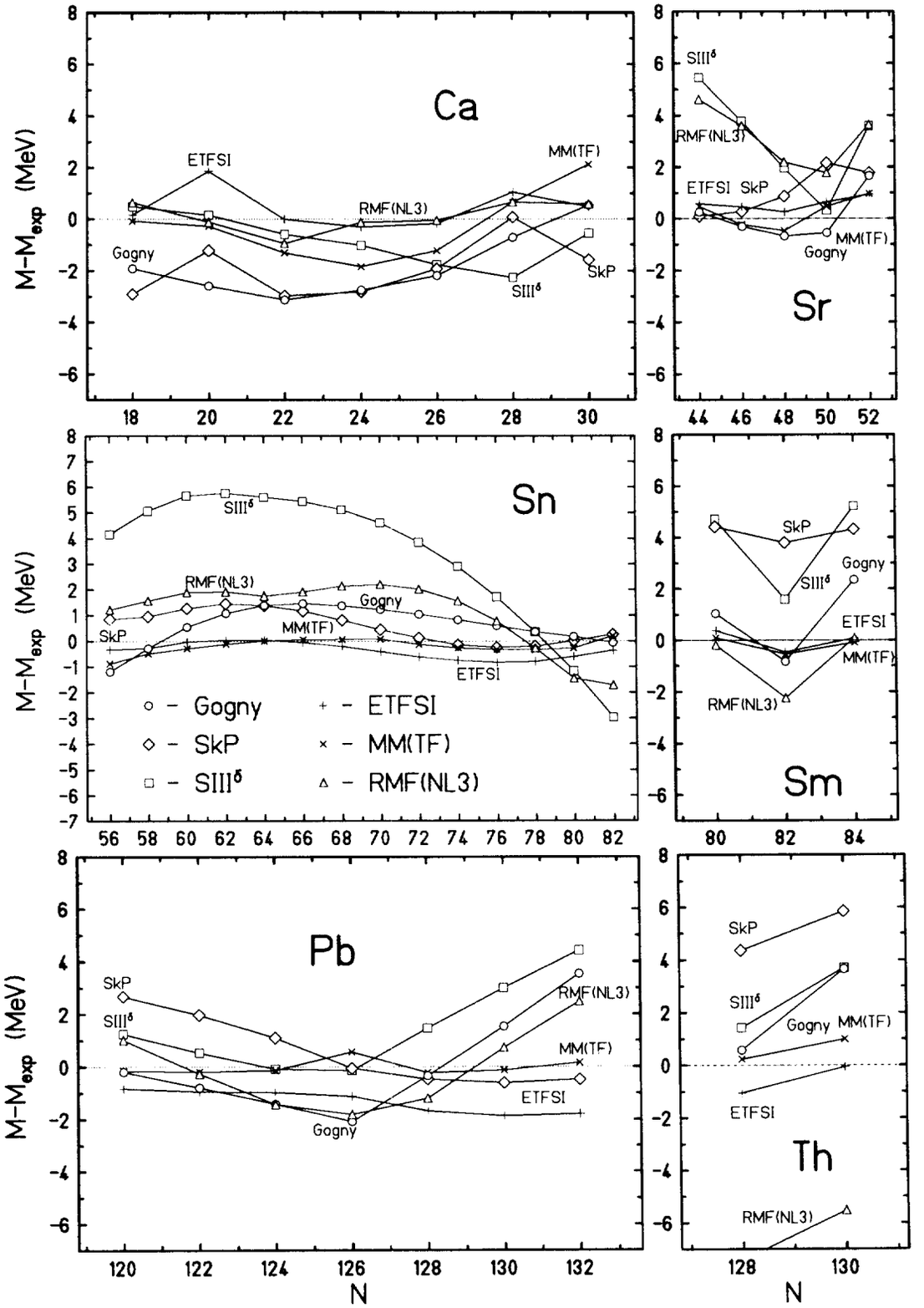

Figure 1: Dependence of the deviation of theoretical mass from the experimental one on the neutron number N, for the elements: Ca, Sr, Sn, Sm, Pb and Th. Six variants of the theoretical mass are considered.

are spherical. Six variants of the calculations are chosen for the illustration.

One can see that the smallest deviations are obtained in the case of the macroscopic-microscopic approach MM(TF), in accordance with the smallest rms value given in Table IV. In this case, the best agreement with experiment is obtained for the heaviest nuclei. Actually, the discrepancy obtained for the Pb and Th isotopes does not exceed 1 MeV (in the absolute value), while it may be as large as about 2 MeV for lighter nuclei (^{44,50}Ca). The results of the ETFSI approach are of about the same quality as those of MM(TF). Here, again, the description of mass is better for heavy nuclei than for the lighter ones.

Among the HFB variants of the calculations, the best description of mass is obtained with the Gogny force. Still, for some nuclei, the deviations may be quite large, about 3 MeV (^{42}Ca) or even more (^{214}Pb). The isotopic dependence of mass, in the Gogny case, is relatively good for some elements (e.g. Sn), while it is much poorer for others. For example, the deviation changes from –2.1 MeV for ^{208}Pb to 3.5 MeV for ^{214}Pb, i.e. by about 5.6 MeV, with the change of N by only 6 units. The quality of the SkP results is similar to that of the Gogny ones. Although rather good for some elements (e.g. Sn), the results may give as large deviations as 4 MeV (Sm isotopes) or even larger (Th isotopes) for other elements. The deviations obtained with the SIII$^{\delta}$ force are rather large. They are as high as about 5 MeV (^{82}Sr, ^{142,146}Sm, ^{214}Pb) or even higher (^{112}Sn). The isotopic dependence of mass obtained with this force is rather poor. The results obtained in the RMF approach (the NL3 variant of parameters) are rather good for the elements Ca, Sn and Sm, but rather bad for Sr and Th.

It is interesting to study the behaviour of mass, obtained in various approaches, when one moves away from the β-stability line. To this aim, we choose nuclei with the proton or neutron numbers equal to one of the four largest magic numbers: $Z = 50, 82$ and $N = 82, 126$. As the experimental mass is not known for many of these nuclei, one of the calculated masses is taken as a reference. We choose the SkP mass for that. The reason is that this mass is calculated in the present analysis and is therefore available for all studied nuclei, but also that the SkP masses reproduce relatively well the experimental values.

To study this dependence of mass on the neutron N and proton Z numbers, far from the β-stability region, we take the same six variants of the calculation as in Fig. 1 and still add one variant more, MM(FRDM), of the macroscopic-microscopic approach. As MM(TF) and MM(FRDM) differ only by the smooth (macroscopic) part of the mass, the difference in their behaviour is just the difference between their macroscopic parts.

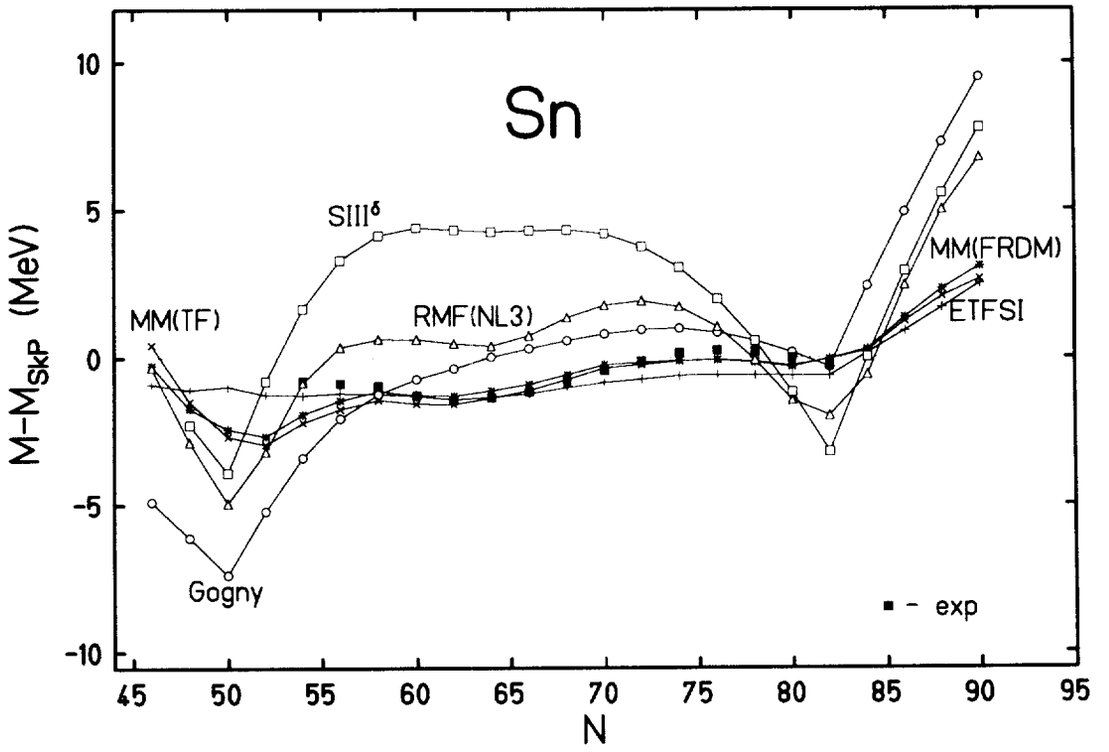

Figure 2: Deviations of various theoretical masses from the SkP mass, calculated for a long chain of Z=50 (Sn) isotopes.

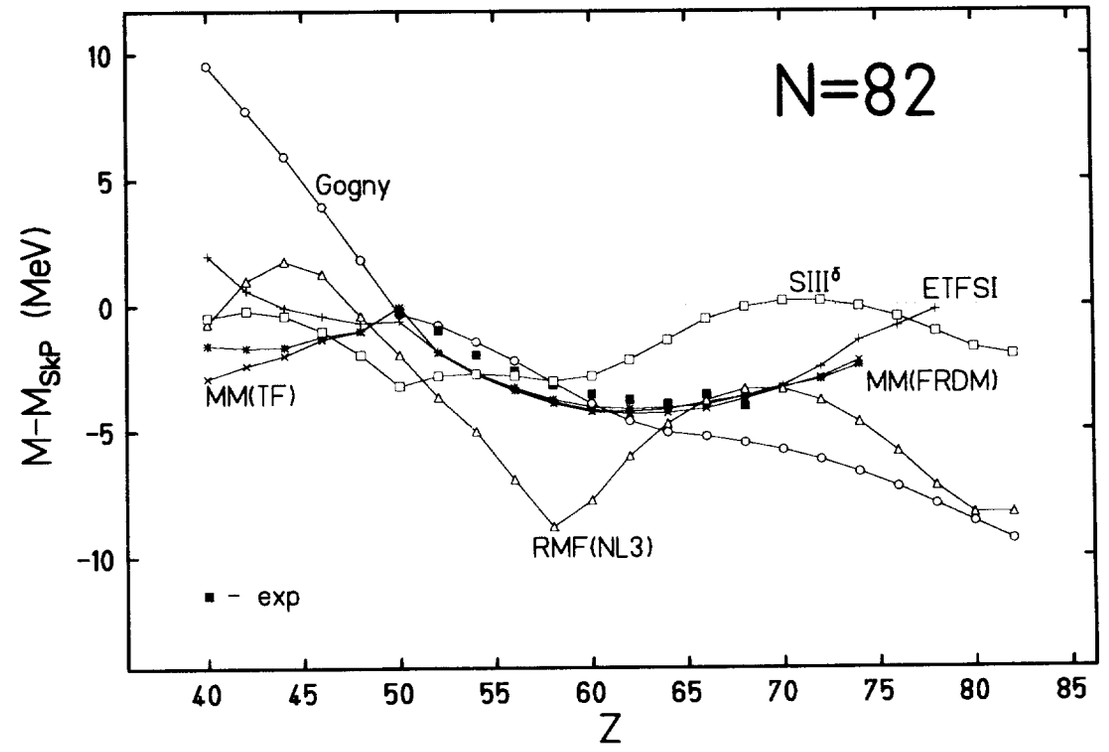

Figure 3: Same as in Fig. 2, but for the N=82 isotones.

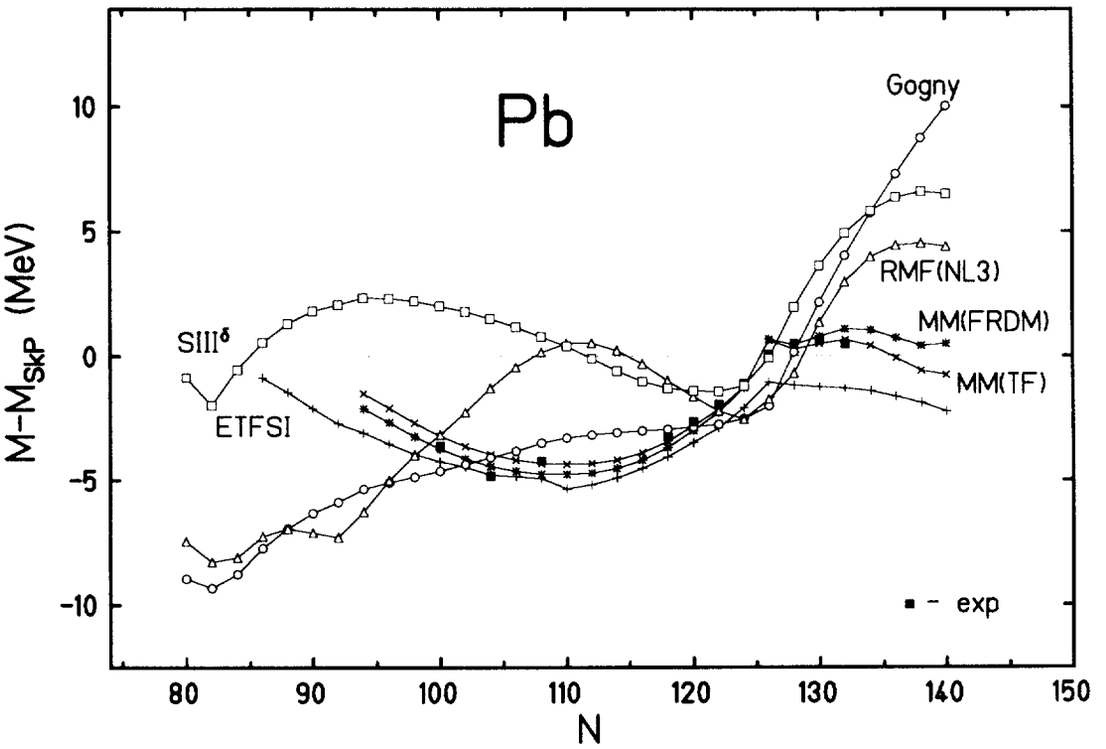

Figure 4: Same as in Fig. 2, but for the Z=82 (Pb) isotopes.

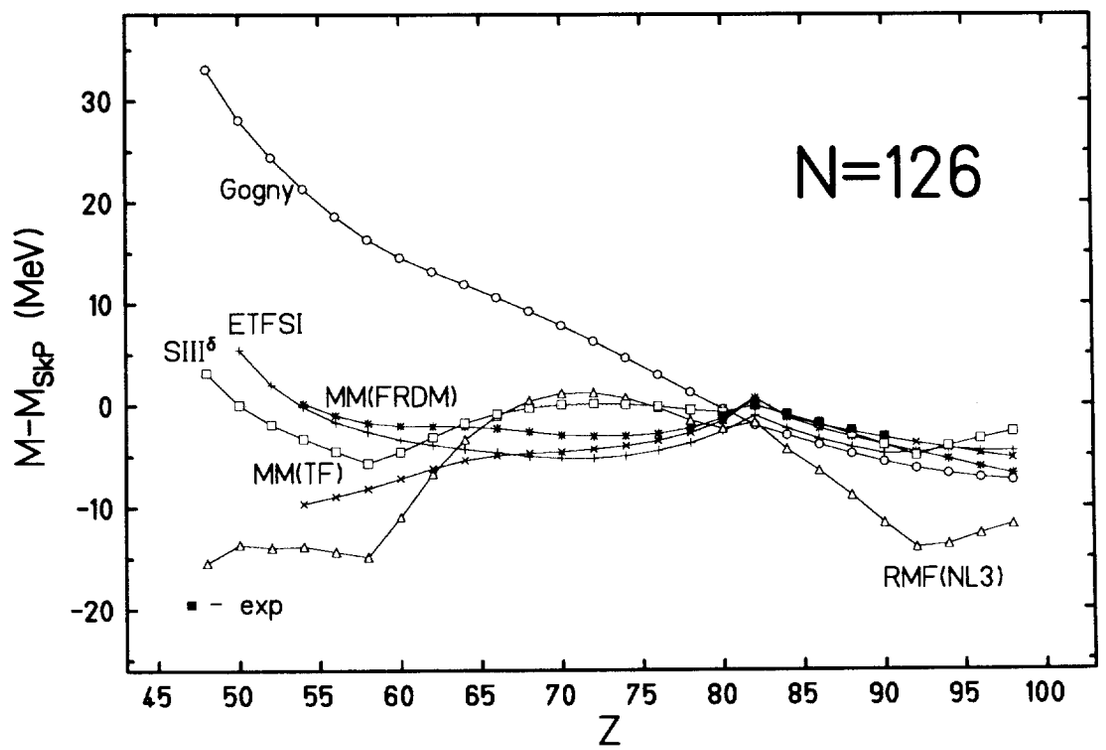

Figure 5: Same as in Fig. 2, but for the N=126 isotones.

Figure 2 shows the mass calculated for nuclides with the proton closed shell at $Z = 50$. This is an extension of the results, shown already in Fig. 1 for the Sn isotopes, to neutron numbers $N < 56$ and also to $N > 82$. One can see that in both these regions of very light and very heavy isotopes, the calculated masses differ much from each other. The Gogny mass is by about 7 MeV smaller for ^{100}Sn and by about 10 MeV larger for ^{140}Sn, than the SkP mass. Both MM masses and the ETFSI mass are relatively close to each other and they are also not very far from the SkP result.

Figure 3 shows the results for isotones with $N = 82$. Here, again, the calculated masses differ much from each other. Again, the difference between the Gogny and SkP masses is very large. The RMF mass differs also much from the SkP mass.

The behaviour of masses for the Pb isotopes is shown in Fig. 4. This is an extension of the results, shown already in Fig. 1, to $N < 120$ and also to $N > 132$. Similarly as in Fig. 3, a large difference in the behaviour of the Gogny and SkP masses is visible.

Finally, Fig. 5 shows the results for the N=126 isotones. The difference of about 30 MeV between the Gogny and SkP masses for ^{176}Sn illustrates the problems which appear when one approaches the neutron drip line. (The nucleus ^{176}Sn is still stable with respect to the separation of one and also of two neutrons, according e.g. to the ETFSI model.)

3.2 Radii

Table V, similar to Table IV, gives the rms values for the difference between the calculated and experimental charge radii. Here, however, the rms is calculated for only 33 spherical nuclei (of 116 nuclei used in Table IV), for which the charge radius has been measured. With respect to Table IV, the MM models are skipped. The experimental values, used to calculate the rms results, are taken from the recent evaluation of experimental data [8].

Table V. Charge–radius rms deviations in fm

SIII:	0.059	SkP:	0.040	SkM*:	0.022
SIII$^{\delta}$:	0.057	SkP$^{\delta}$:	0.033	SkM*$^{\delta}$:	0.021
SIII$^{\delta\rho}$:	0.065	SkP$^{\delta\rho}$:	0.043	SkM*$^{\delta\rho}$:	0.023
Gogny:	0.031				
RMF(NL1):	0.026	RMF(NL2):	0.031	RMF(NL3):	0.028
ETFSI:	0.021				

One can see that the best description of the charge radii is obtained within the ETFSI model and for the HFB calculations with the SkM*$^{\delta}$ force. The results with the SkM* force are very good almost independently of the interaction used to generate the pairing correlations. Relatively good results are also obtained in the RMF calculations with the NL1 and NL3 parameters. With the NL2 parametrization, the results are slightly worse, similar to those obtained in the HFB approach with the Gogny and SkP$^{\delta}$ forces. The largest rms values are obtained with the SIII force, independently of the variant of the pairing interaction used.

Figure 6 illustrates the dependence of the discrepancy between the calculated values of the charge radius and the experimental ones on the neutron number N, for three elements: Ca, Sn and Pb. These are the elements, for which most experimental values are available. The same variants of the calculations are taken for the illustration as in Fig. 1, with the exception that the macroscopic-microscopic values are skipped, as mentioned already above. One can see that the dependence

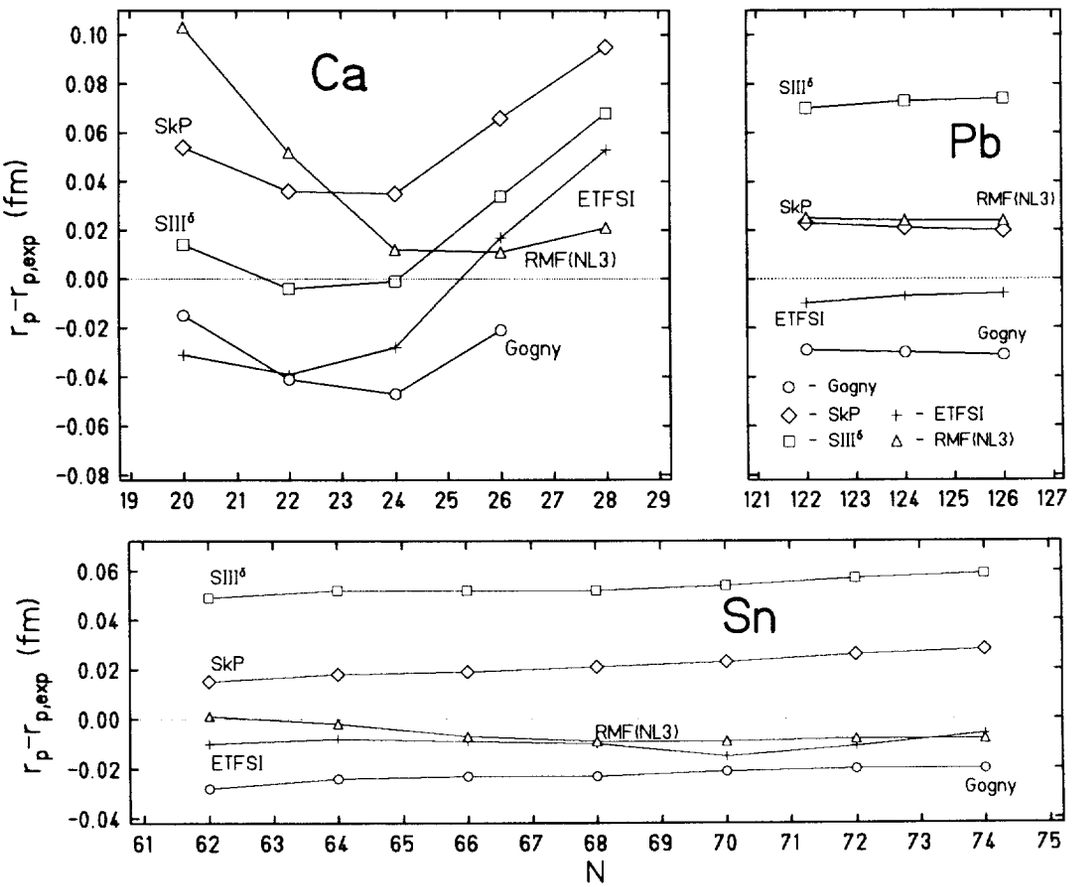

Figure 6: Dependence of the deviation of theoretical charge radius from the experimental one on the neutron number N, for the elements: Ca, Sn and Pb. Five variants of the theoretical radius are considered.

of the discrepancy is rather weak for Sn and Pb, i.e.,that the calculations correctly reproduce the isotopic dependence of the radius for these two (heavy) elements.

When one moves away from the β-stability line, the differences between proton (or charge), $r_{\rm p}$, and neutron (neutron-matter), $r_{\rm n}$, radii increase. Within the HFB approximation with the Skyrme forces, this effect has recently been studied in [42]. Here, we present results obtained within the RMF approach (NL3 variant) and within the HFB theory with the Gogny force, and compare them with the SkP results [42].

Figures 7–10 show results obtained for the the same chains of nuclei as used in Figs. 2–5. Results of the three variants of the calculations: HFB with the Gogny and SkP forces and the RMF(NL3) variant, are shown.

One can see in Fig. 7 that for light isotopes of tin (like ^{96}Sn), the neutron radius is by up to about 0.27 fm smaller, and for heavy isotopes (like ^{140}Sn) it is by up to about 0.48 fm larger, than the proton radius. For stable isotopes ^{116}Sn and ^{124}Sn, for which both these radii are measured, the experimental value of $r_{\rm n}$ is larger than that of $r_{\rm p}$ by 0.064 fm and 0.176 fm, respectively. The isotope, for which these two radii are expected to be equal, is ^{110}Sn or ^{112}Sn, depending on the variant of the calculation.

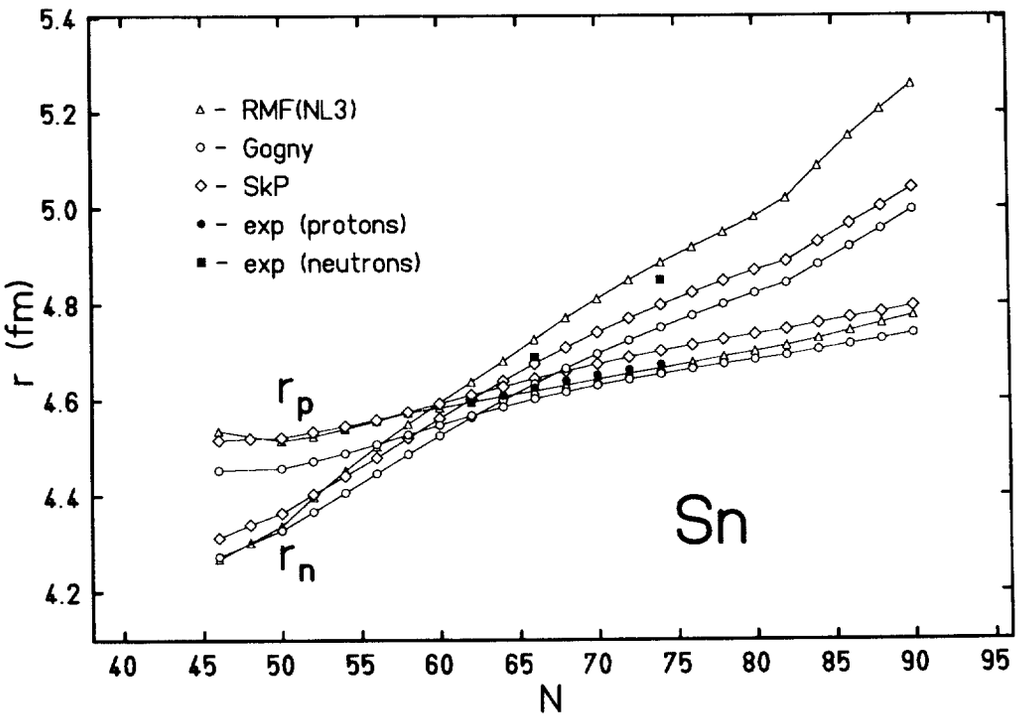

Figure 7: Charge and neutron-matter radii calculated for a long chain of Z=52 (Sn) isotopes. Three variants of the calculations are considered. Experimental values are also shown, for comparison.

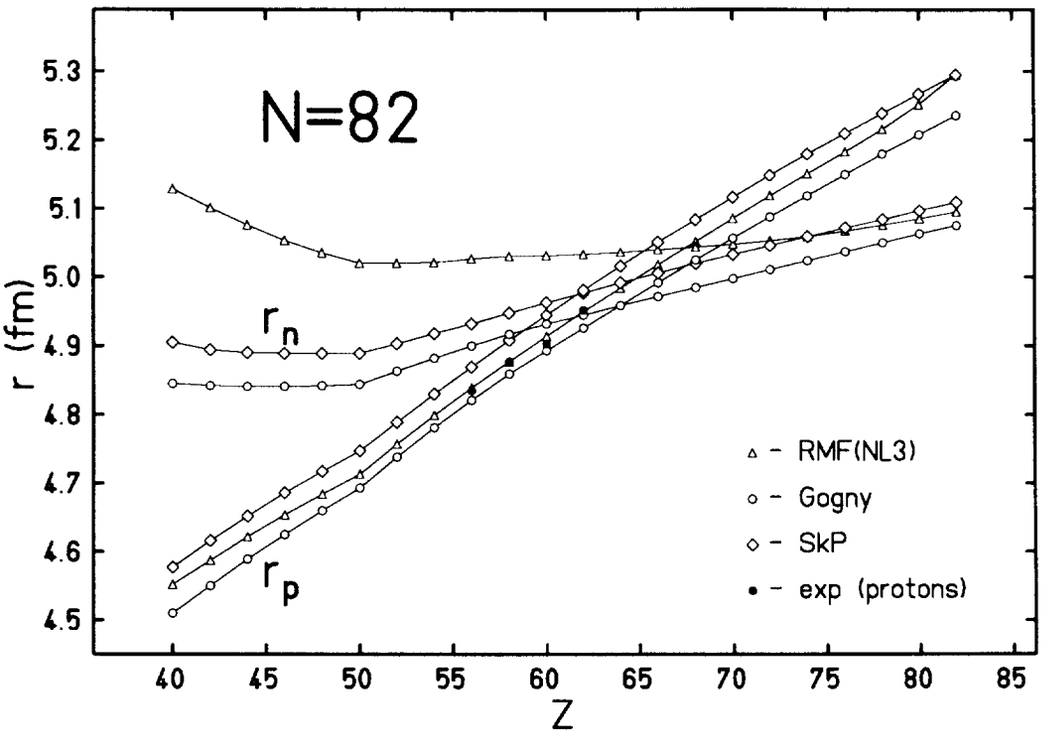

Figure 8: Same as in Fig. 7, but for the N=82 isotones.

It is seen in Fig. 8 that for such a neutron-rich nucleus as ^{122}Zr, r_n may be larger than r_p by up to about 0.58 fm. The difference 0.58 fm is obtained in the RMF(NL3) calculation. The nucleus ^{122}Zr is expected to be close to the neutron drip line (according, e.g., to the ETFSI model).

Figure 9 shows that the experimental values of r_n and r_p for ^{208}Pb differ by 0.085 fm. The nucleus, for which these radii are expected to be about equal, is much lighter. This is the isotope: ^{188}Pb in the Gogny, ^{190}Pb in the SkP, and ^{182}Pb in the RMF(NL3) calculations, respectively. Especially large difference between r_n and r_p is obtained for neutron-rich isotones with N=126 (Fig. 10). It is about 0.52 fm in the Gogny, about 0.77 fm in the SkP and about 0.86 fm in the RMF(NL3) calculations, for the nucleus ^{176}Sn. These two radii are expected to be about equal only at about the heavy end of this chain, around the neutron-deficient nucleus: ^{218}U, ^{220}Pu or ^{226}Fm, depending on the variant of the calculation.

A comparison between the considered approaches shows that apart from the immediate vicinity of the neutron drip line, results obtained within the HFB theory with the SkP and Gogny forces are very similar; isotopic trends are almost identical and the only difference between these two approaches is a systematic offset of about 0.05 fm which makes the radii obtained for the Gogny force slightly smaller. As discussed in [42] and illustrated also here, very close to the neutron drip line the

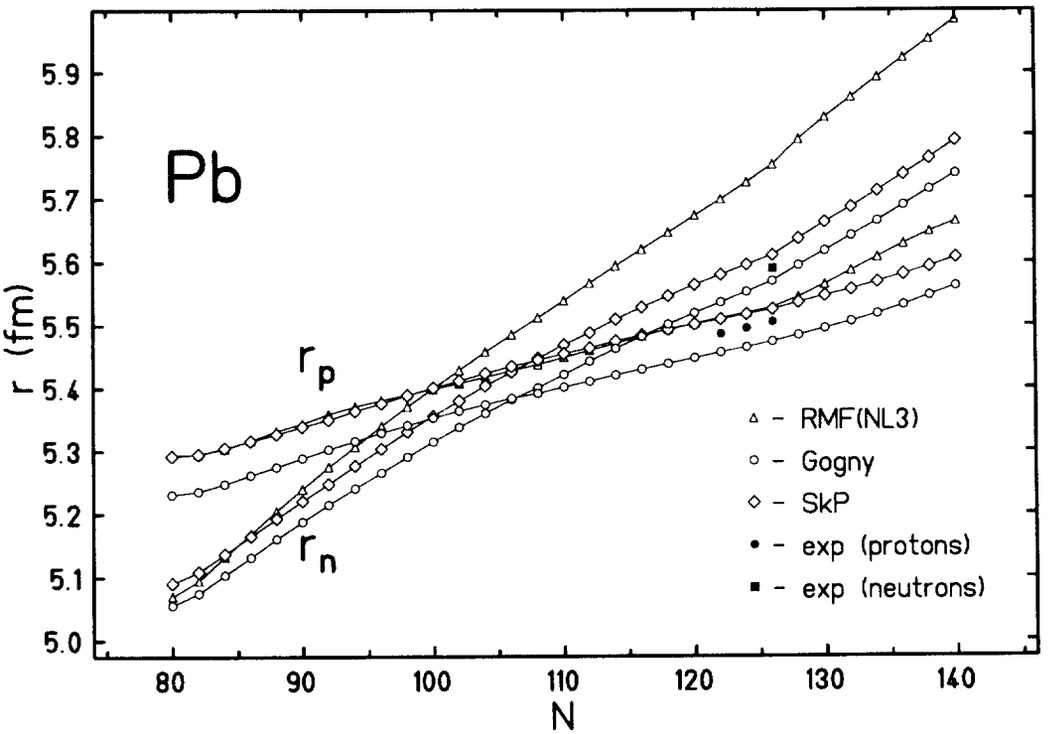

Figure 9: Same as in Fig. 7, but for the Z=82 (Pb) isotopes.

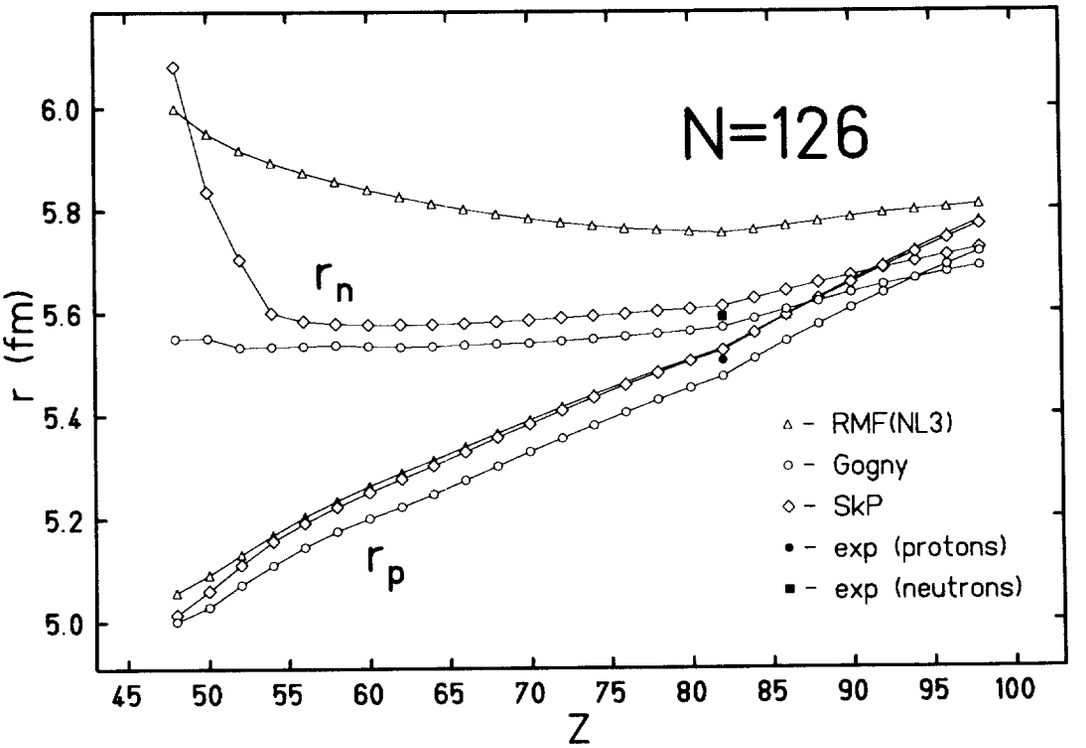

Figure 10: Same as in Fig. 7, but for the N=126 isotones.

SkP force gives sudden increase of the radius. This effect occurs because the neutron distributions extend in these nuclei to large distances. It is not clear at the moment whether the other forces can give similar results, because such a question can only be answered by solving corresponding self-consistent equations in space coordinates.

The isotopic dependencies of the charge radii are similar in all three presented theories. However, for neutron radii one obtains in the RMF approach with the NL3 interaction a much faster increase with the neutron number than in the other two theories. Since the neutron radii have been measured for two tin isotopes, ^{116}Sn and ^{124}Sn, we can conclude that here the RMF results are in a better agreement with data than the HFB results. On the other hand, in the ^{208}Pb nucleus the difference between neutron and proton radius is overestimated by the RMF approach by about a factor of two, while it is correctly accounted for by the HFB theory. Clearly, a significant increase in the number of available experimental data for neutron radii is needed before a more conclusive evaluation of theoretical results can be made.

4 Conclusions

The following conclusions may be drawn from our study:

(1) The best description of mass of the considered nuclei is obtained in the macroscopic-microscopic approach. The description by the ETFSI model is, however, of a similar quality. In both descriptions, the agreement with experimental values is better for heavy than for light nuclei.

(2) Among the self-consistent Hartree-Fock-Bogoliubov descriptions, the variant using finite-range Gogny effective interaction gives the best results. The quality of the variant making use of the Skyrme SkP force is, however, similar. The results obtained with the SIII force, which has been used for a long time in the calculations of various nuclear properties, are worse. The isotopic dependence of mass, obtained with the SIII force, is also rather poor.

(3) Within the Relativistic Mean Field approach, a significant improvement of the description of masses has been obtained with the very recent set of parameters NL3. The quality of this description is similar to that of the HFB approach with the SkP force.

(4) It seems that a better description of masses could be obtained, both in the HFB and RMF approaches, if more data (i.e., masses of more nuclei) would be used in the adjustment of free parameters. It should also be stressed that in neither of these theories the existing parameters have been determined with a focus on masses, as has been done in the MM or ETFSI methods.

(5) The discrepancy between various approaches, in predictions of nuclear masses,

becomes especially large when one moves off the β-stability line. For example, the Gogny mass is by about 7 MeV smaller for ^{100}Sn and by about 10 MeV larger for ^{140}Sn than the SkP mass, although these two nuclei are not very far from the experimental region. For a more neutron-rich nucleus, like ^{186}Nd, this difference increases to about 15 MeV, and it further increases to about 30 MeV for the nucleus ^{176}Sn. This illustrates the difficulties in predicting nuclear masses when one approaches the neutron drip line.

(6) Nuclear charge radius is best described by the ETFSI model and by the HFB calculations with the SkM* forces. The description by the RMF method with the NL1 and NL3 parameters is not much worse. Similarly as for mass, the description is generally better for heavy nuclei than for lighter ones.

(7) For nuclei far from β-stabilty, the calculated proton and neutron radii much differ. For example, for light isotopes of Sn (like ^{96}Sn), the neutron radius is by up to about 0.27 fm smaller, and for heavy isotopes (like ^{140}Sn) it is by up to about 0.48 fm larger, than the proton radius. For still more neutron-rich isotopes (like ^{176}Sn), $r_{\rm n}$ is obtained larger than $r_{\rm p}$ by up to about 0.86 fm.

(8) While for lighter elements, the nuclei, for which $r_{\rm p}$ is about equal to $r_{\rm n}$, are situated in the β-stability region, they are expected to be rather far from this region for heavy elements. For example, for Sn isotopes, such nuclei are obtained to be ^{110}Sn or ^{112}Sn, depending on the variant of the calculation, i.e. on the border of β stability (^{112}Sn is the lightest isotope which is β stable). For the N=126 isotones, the relation $r_p \approx r_n$ is obtained for ^{218}U (in the SkP variant), ^{220}Pu (the Gogny case) or ^{226}Fm (the RMF(NL3) calculation). Thus, the approximate equality of these two radii is expected to appear for the very neutron-deficient nuclei, removed from the β-stability region by about 16 mass units or more.

(9) Neutron radii increase with neutron number much faster in the RMF approach than in the HFB theories. More experimental data are definitely needed before one can conclude whether this fact characterizes the particular forces used or illustrates more profound features of the theoretical description.

The authors would like to thank H. Flocard and P. Quentin for useful discussions and suggestions during the early stage of this study. They would also like to thank P. Armbruster, H. Geissel, S. Hofmann, H.-J. Kluge, C. Kozhuharov, G. Münzenberg and W. Nörenberg for helpful discussions. Support by the Polish Committee for Scientific Research (KBN), Grants no. 2 P03B 156 08, 2 P03B 049 09, and 2 P03B 034 08, is gratefully acknowledged.

References

[1] *Proc. Int. Conf. on Exotic Nuclei and Atomic Masses*: "ENAM 95", Arles (France) 1995, edited by M. de Saint Simon and O. Sorlin (Editions Frontieres, Gif-sur-Yvette, 1995).

[2] T. Radon, Th. Kerscher, B. Schlitt, K. Beckert, T. Beha, F. Bosch, H. Eickhoff, B. Franzke, Y. Fujita, H. Geissel, M. Hausmann, H. Irnich, H. C. Jung, O. Klepper, H.-J. Kluge, C. Kozhuharov, G. Kraus, K. E. G. Löbner, G. Münzenberg, Yu. Novikov, F. Nickel, F. Nolden, Z. Patyk, H. Reich, C. Scheidenberger, W. Schwab, M. Steck, K. Sümmerer and H. Wollnik, *Phys. Rev. Lett.* **78**, 4701 (1997).

[3] *Proceedings of the International Workshop on the Physics and Techniques of Secondary Nuclear Beams*, Dourdan (France) 1992, edited by J.F. Bruandet, B. Fernandez and M. Bex (Editions Frontieres, Gif-sur-Yvette, 1992).

[4] *Proceedings of the International Workshop*: "Research with Fission Fragments", Benediktbeuern (Germany) 1996 (World Scientific, Singapore, 1997).

[5] I. Tanihata, *Heavy Ion Physics* **5**, 000 (1997).

[6] T. Otto, G. Bollen, G. Savard, L. Schweikhard, H. Stolzenberg, G. Audi, R.B. Moore, G. Rouleau, J. Szerypo and Z. Patyk, *Nucl. Phys.* **A567**, 281 (1994).

[7] E.W. Otten, in Treatise on Heavy-Ion Physics, vol. 8, edited by D.A. Bromley (Plenum, New York, 1989) p. 517

[8] E.G. Nadjakov, K.P. Marinova and Yu.P. Gangrsky, *At. Data Nucl. Data Tables* **56**, 133 (1994).

[9] Z. Patyk, A. Baran, J.F. Berger, J. Dechargé, J. Dobaczewski, R. Smolańczuk and A. Sobiczewski, *Acta Phys. Pol.* **B27**, 457 (1996).

[10] T.H.R. Skyrme, *Phil. Mag.* **1**, 1043 (1956).

[11] J. Bartel, P. Quentin, M. Brack, C. Guet and H.B. Håkansson, *Nucl. Phys.* **A386**, 79 (1982).

[12] P. Bonche, H. Flocard, P.H. Heenen, S.J. Krieger and M.S. Weiss, *Nucl. Phys.* **A443**, 39 (1985).

[13] M. Beiner, H. Flocard, Nguyen Van Giai and P. Quentin, *Nucl. Phys.* **A238**, 29 (1975).

[14] H. Flocard, P. Quentin, D. Vautherin, M. Veneroni and A.K. Kerman, *Nucl. Phys.* **A231**, 176 (1974).

[15] H. Krivine, J. Treiner and O. Bohigas, *Nucl. Phys.* **A336**, 155 (1980).

[16] J. Dobaczewski, H. Flocard and J. Treiner, *Nucl. Phys.* **A422**, 103 (1984).

[17] E. Chabanat, Ph.D. Thesis, Report 1695 (IPN, Lyon, 1995).

[18] E. Chabanat, P. Bonche, P. Haensel, J. Meyer and R. Schaeffer, *Phys. Scr.* **T56**, 231 (1995).

[19] J. Dobaczewski, W. Nazarewicz and T.R. Werner, *Phys. Scr.* **T56**, 15 (1995).

[20] J. Dobaczewski, W. Nazarewicz, T.R. Werner, J.-F. Berger, C.R. Chinn and J.Dechargé, Phys. Rev **C53**, 2809 (1996).

[21] D. Gogny, Proc. Int. Conf. on Nuclear Physics, eds. J. de Boer and H.J. Mang (North Holland, Amsterdam, 1973) p. 48.

[22] J. Dechargé and D. Gogny, *Phys. Rev.* **C21**, 1568 (1980).

[23] J.F. Berger, M. Girod and D. Gogny, *Nucl. Phys.* **A502**, 85c (1989).

[24] J.F. Berger, M. Girod and D. Gogny, *Comput. Phys. Commun.* **63**, 365 (1991).

[25] J.F. Berger, in *Proceedings of the International Conference on Nuclear Shapes and Nuclear structure at Low Excitation Energies*, Antibes (France) 1994, edited by M. Vergnes, D. Goutte, P.H. Heenen and J. Sauvage (Editions Frontieres, Gif-sur-Yvette, 1994) p. 1.

[26] J.F. Berger, L. Bitaud, J. Decharge, M. Girod and S. Peru-Desenfants, in *Proceedings of the International Workshop*: "Extremes of Nuclear Structure", Hirschegg (Austria) 1996, edited by H. Feldmeier, J. Knoll and W. Nörenberg (GSI, Darmstadt, 1996) p. 43.

[27] Y. Aboussir, J.M. Pearson, A.K. Dutta and F. Tondeur, *Nucl. Phys.* **A549**, 155 (1992).

[28] Y. Aboussir, J.M. Pearson, A.K. Dutta and F. Tondeur, *At. Data Nucl. Data Tables* **61**, 127 (1995).

[29] B.D. Serot and J.D. Walecka, *Adv. Nucl. Phys.* **16**, 1 (1986).

[30] P.-G. Reinhard, *Rep. Prog. Phys.* **52**, 439 (1989).

[31] Y.K. Gambhir, P. Ring and A. Thimet, *Ann. Phys. (N.Y.)* **198**, 132 (1990).

[32] A. Baran, J.L. Egido, B. Nerlo-Pomorska, K. Pomorski, P. Ring and L.M. Robledo, *J. Phys.* **G21**, 657 (1995).

[33] P. Ring, *Prog. Part. Nucl. Phys.* **37**, 193 (1996).

[34] P.-G. Reinhard, M. Rufa, J. Maruhn, W. Greiner and J. Friedrich, *Z. Phys.* **A323**, 13 (1986).

[35] S.J. Lee, J. Fink, A.B. Balantekin, M.R. Strayer, A.S Umar, P.G. Reinhard, J.A. Maruhn and W. Greiner, *Phys. Rev. Lett.* **57**, 2916 (1986).

[36] G.A. Lalazissis, J. König and P. Ring, *Phys. Rev.* **C55**, 540 (1997).

[37] P. Möller, J.R. Nix, W.D. Myers and W.J. Swiatecki, *At. Data Nucl. Data Tables* **59**, 185 (1995).

[38] W.D. Myers and W.J. Swiatecki, *Nucl. Phys.* **A601**, 141 (1996).

[39] W.D. Myers and W.J. Swiatecki, *Ann. Phys. (N.Y.)* **55**, 395 (1969).

[40] M.M. Sharma, M.A. Nagarajan and P. Ring, *Phys. Lett.* **B312**, 377 (1993).

[41] G. Audi and A.H. Wapstra, *Nucl. Phys.* **A595**, 409 (1995).

[42] J. Dobaczewski, W. Nazarewicz, and T.R. Werner, *Z. Phys.* **A354**, 27 (1996).